RESEARCH ARTICLE | SEPTEMBER 08 2026

Zr-related states in AlN probed by photocurrent excitation spectroscopy

F. A. Rafi ; H. Alwan ; J. Li ; J. Y. Lin ; H. X. Jiang

Appl. Phys. Lett. 129, 101902 (2026)
https://doi.org/10.1063/5.0347982

Applied Physics Letters ARTICLE pubs.aip.org/aip/apl

Zr-related states in AlN probed by photocurrent excitation spectroscopy

Cite as: Appl. Phys. Lett. **129**, 101902 (2026); doi: 10.1063/5.0347982
Submitted: 14 June 2026 · Accepted: 20 August 2026 ·
Published Online: 8 September 2026

F. A. Rafi, H. Alwan, J. Li, J. Y. Lin, and H. X. Jiang[a]

AFFILIATIONS

Department of Electrical and Computer Engineering, Texas Tech University, Lubbock, Texas 79409, USA

[a]Author to whom correspondence should be addressed: hx.jiang@ttu.edu

ABSTRACT

Zirconium (Zr) is predicted and experimentally confirmed to substitute on the Al site (Zr_{Al}), where it acts as a deep donor approximately 1.5 eV below the conduction band minimum in aluminum nitride (AlN). Furthermore, the neutral zirconium-nitrogen vacancy complex, $(Zr_{Al}–V_N)^0$, has been predicted to be an attractive candidate for room-temperature qubits. In this work, Zr-doped AlN epilayers were synthesized on AlN bulk substrates via metal-organic chemical vapor deposition. Structural and morphological characterizations confirmed excellent crystalline orientation and sub-nanometer surface roughness. While photoluminescence spectra were dominated by vacancy-impurity complexes, photocurrent excitation spectroscopy effectively mapped Zr-related states. Specifically, an isolated donor level was resolved at 1.5 eV alongside $(Zr_{Al}–V_N)^{0/1-}$ complex configurations near 2 and 3 eV. Each complex exhibits a distinct 0.2 eV doublet splitting driven by π-bonding and σ-bonding configurations within the wurtzite lattice. These findings provide experimental confirmation of the deep-level electronic properties of Zr in AlN, establishing a framework for the development of extrinsic photoconductive semiconductor switches and room-temperature qubit applications.

Ultrawide-bandgap (UWBG) AlN semiconductor is indispensable in the development of next-generation deep UV optoelectronics,[1–6] high-power electronics,[7–12] and quantum information technologies.[13–15] This potential stems from its direct UWBG of 6.1 eV,[1,16] high thermal conductivity (320 W/m K),[17–19] large electron mobility ($\mu_e > 400\,cm^2/V\,s$),[20] and the largest critical electric field among all semiconductors (15 MV/cm).[21]

Transition metals, specifically zirconium (Zr), are predicted[13] and experimentally verified[22] to substitute on the Al site (Zr_{Al}) and act as deep donors located approximately 1.4 eV below the conduction band minimum (CBM).[13] Furthermore, the neutral zirconium-nitrogen vacancy complex, $(Zr_{Al}–V_N)^0$, has been predicted to support localized quantum states that decouple from delocalized conduction band states, making Zr-doped AlN (AlN:Zr) an attractive candidate for applications in room-temperature qubits.[13] Other than the potential applications of AlN:Zr for qubits, AlN:Zr appears to be a compelling platform for the development of optically triggered high-power/high voltage switch devices, such as extrinsic photoconductive semiconductor switches (PCSSs), which bypass the doping challenges for realizing AlN p-n junction electronic switching devices. However, the ability of introducing deep-level Zr dopants into AlN is crucial for extrinsic PCSS operation, as such an approach would yield an extremely low leakage current in the off-state (dark state) while simultaneously enabling high current/power operation using sub-bandgap optical triggering in the on-state via compact and mature laser diodes.

Despite these promising prospects, experimental mapping of Zr-related impurity energy levels in AlN has remained elusive. Photoluminescence (PL) spectroscopy often fails to deterministically resolve these states due to dominant transitions related to other native defects in AlN:Zr.[14,15,23] In this work, we employ photocurrent excitation spectroscopy (PES) to overcome these limitations. Because PES selectively records free carrier generation via band-to-band or impurity-to-band transitions, it effectively precludes donor–acceptor pair and pure intra-defect transitions. Pertaining to Zr-related impurity states, a previous theoretical study[13] has predicted the following: (1) The isolated Zr_{Al} donor level is about 1.4 eV below the CBM with this line expected to be observable in PES; (2) The optical energies required to excite an electron bound to $(Zr_{Al}–V_N)^0$ to the CBM are near 4.97 and 3.07 eV with corresponding emission energies near 3.78 and 2.11 eV for the spin-minority excitation and spin-majority excitation, respectively, which are also expected to be observable in PES; (3) The excitation energy of the intra-defect transition involving $(Zr_{Al}–V_N)^0$ is near 2.83 eV with a corresponding emission energy near 1.91 eV, and this line is not expected to be observable in PES since it originates from the internal (or intra-defect) transition within

$(Zr_{Al}–V_N)^0$. Previous experimental results related to Zr levels in AlN include: (1) A broad optical absorption peak near 1.78 eV was attributed to optical excitation of an electron bound to a negatively charged complex of $(Zr_{Al}–V_N)^{-1}$ to the CBM;[23] (2) A PL emission peak near 2.46 eV was attributed to the recombination of a conduction electron with a $(Zr_{Al}–V_N)$ complex, described by the process of $e^- + (Zr_{Al}–V_N)^+ \rightarrow (Zr_{Al}–V_N)^0 + h\nu$ (2.46 eV),[23] compared to a predicted value of 2.11 eV;[13] (3) PL emission spectroscopy studies also observed possible intra-defect transition within $(Zr_{Al}–V_N)^0$ near 1.7 eV (Ref. 14) and 1.8 eV (Ref. 23) compared to a predicted value of 1.91 eV,[13] which is not expected to be observable in PES. Emission and absorption energies typically differ due to the lattice relaxation associated with these defect-impurity complexes.

Undoped AlN and AlN:Zr epilayers were grown via metal-organic chemical vapor deposition (MOCVD) on *c*-plane bulk AlN substrates. Trimethylaluminum (TMA) and ammonia (NH_3) served as the Al and N precursors, respectively. Tetrakis(dimethylamino) zirconium (TDMAZr) was supplied to the reactor as the Zr precursor using H_2 as the carrier gas. Growth was initiated by directly depositing a 10 μm thick undoped AlN or AlN:Zr epilayer on the substrate at a growth temperature of 1250 °C. Schematic layer structures of the undoped AlN and AlN:Zr epilayers are illustrated in the insets of Fig. 1(a).

Surface morphology and crystalline quality were evaluated using atomic force microscopy (AFM) and x-ray diffraction (XRD) rocking curves. The XRD (002) rocking curves [Fig. 1(a)] exhibit well-defined, sharp symmetric peaks for both samples, confirming highly aligned c-axis epitaxial growth. The full-width at half-maximum (FWHM) of the AlN:Zr sample is 70 arc sec compared to 20 arc sec for the undoped reference. This moderate broadening is expected, arising from local lattice perturbations introduced by the atomic size discrepancy of intentional Zr incorporation. As shown in Fig. 1(b), the AlN:Zr epilayer maintains a highly smooth surface with a root mean square (RMS) roughness of 0.25 nm, which is comparable to the 0.18 nm measured for the undoped AlN reference. This sub-nanometer roughness confirms that intentional Zr incorporation at levels up to 3.3×10^{19} cm^{-3} does not degrade the surface morphology, preserving conformability with photolithography and contact metallization processing. Figure 1(c) plots Zr and O concentrations in AlN:Zr epilayer probed by secondary ion mass spectrometry (SIMS). The results revealed that the Zr concentration is 3.3×10^{19} cm^{-3}, which is about two orders of magnitude higher than that of unintentional oxygen impurities (5×10^{17} cm^{-3}).

Room-temperature PL spectra under above-bandgap excitation by an excimer laser are shown in Fig. 2. The undoped AlN reference (Fig. 2, inset) is dominated by a sharp band-edge emission at ~5.9 eV, showcasing excellent crystal and optical quality. Upon Zr doping, the near band-edge emission is significantly quenched, and a broad, deep-level band centered around 3.6 eV becomes the dominant feature. The emission band occurring in the energy range of 3.4–3.6 eV is well known in AlN and is commonly assigned to the recombination of Al vacancies (V_{Al}) and their complexes with oxygen impurities, more specifically to the band-to-impurity recombination involving $(V_{Al}–2O_N)^{0/1-}$ and $(V_{Al}–O_N)^{2-/1-}$ defect complexes.[24–26] Theoretical work suggested that $(Zr_{Al}–V_N)^0$ complex produces localized intra-defect emission lines around 1.91 and 3.78 eV.[13] However, these features cannot be resolved in the PL spectrum of Fig. 2 because carrier recombination pathways through the ubiquitous complexes are overwhelmingly dominant under above-bandgap optical pumping.

To gain insight into the formation of Zr donor impurities and defect complexes during growth, it is important to bear in mind that Zr_{Al} is a simple donor, though it is quite deep with a calculated energy

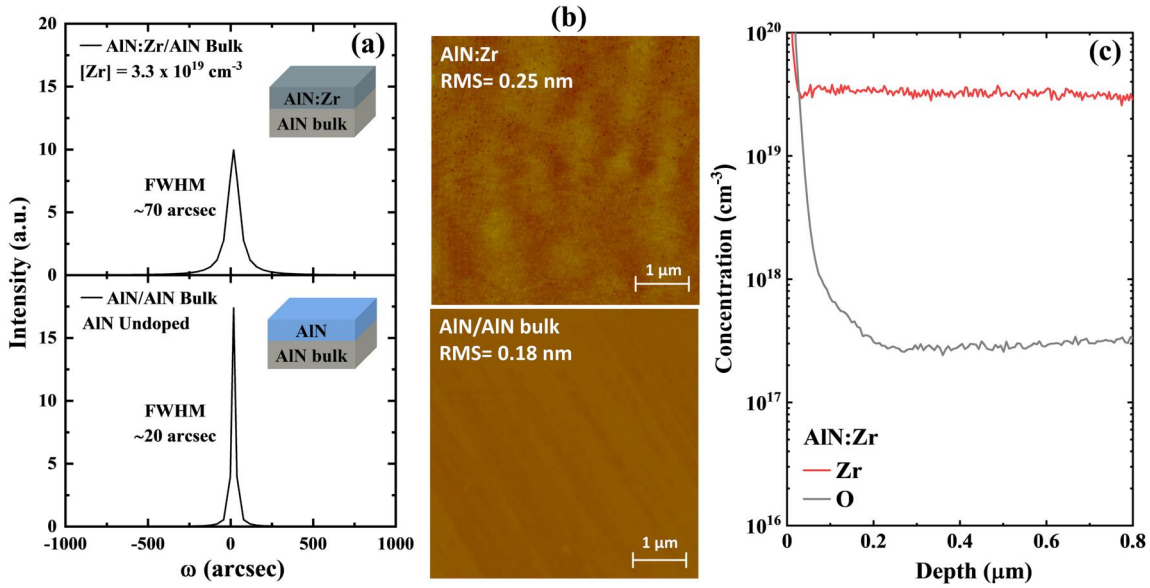

FIG. 1. (a) XRD (002) ω-rocking curves and (b) AFM surface morphology of 10 μm thick Zr-doped AlN (AlN:Zr) and undoped AlN epilayers. The measured RMS roughness values are 0.25 and 0.18 nm over a 5 × 5 μm^2 area, and the corresponding rocking-curve FWHM values are about 70 and 20 arc sec. Schematic layer structures of undoped AlN and AlN:Zr epilayers are illustrated in the insets of (a). (c) Concentrations of Zr and O in AlN:Zr sample probed by SIMS.

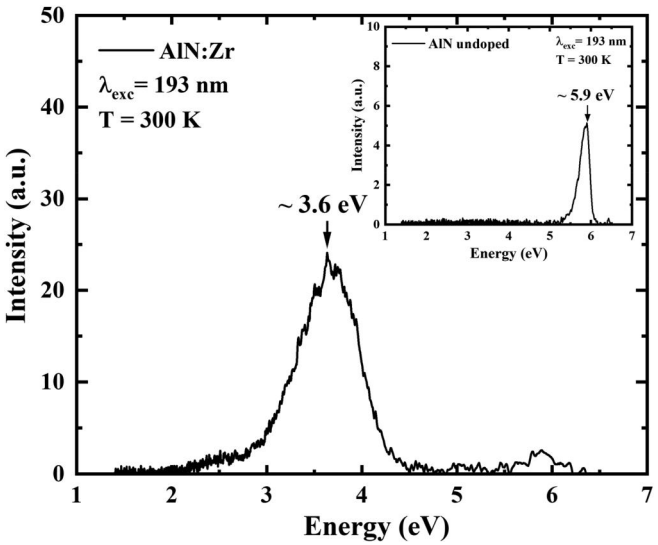

FIG. 2. Room-temperature (T = 300 K) PL spectrum of AlN:Zr epilayer excited by an excimer laser (λ_{exc} = 193 nm). The inset plots the PL spectrum of an undoped AlN epilayer measured under identical conditions.

level of about 1.4 eV below the CBM.[13] At a growth temperature of 1250 °C (or 1523 K) (kT ~ 0.127 eV), the fraction of ionized Zr_{Al} can be estimated to be about $\exp\left(\frac{-1.4\,eV}{0.127\,eV}\right) \approx 1.6 \times 10^{-5}$. This indicates that the vast majority of Zr_{Al} donors remain in a neutral charge state, pinning the Fermi level at the Zr_{Al} donor level, located about 1.4 eV below the CBM.[13] Furthermore, previous theoretical results[13] revealed two critical insights. First, the formation energies of Zr_{Al}–V_N complexes are comparable to those of isolated Zr_{Al} donors, implying that their resulting concentrations are also comparable. Second, with the Fermi level pinned at the energy level of Zr_{Al} donor, a greater proportion of negatively charged complexes $(Zr_{Al}–V_N)^{-1}$ are formed during growth compared to neutral ones $(Zr_{Al}–V_N)^0$ because the energy level of $(Zr_{Al}–V_N)^{-1}$ lies below that of Zr_{Al} donors. Consequently, the system ends up with more neutral Zr_{Al} donors than positively charged ones ($Zr^0_{Al} > Zr^+_{Al}$) and more negatively charged complexes than neutral ones $[(Zr_{Al}–V_N)^{-1} > (Zr_{Al}–V_N)^0]$. Nonetheless, Zr^0_{Al}, $(Zr_{Al}–V_N)^{-1}$, and $(Zr_{Al}–V_N)^0$ can all contribute to photocurrent under illumination with correct excitation energies.

To resolve Zr-related states, PES measurements were performed at room temperature. Peaks in a PES represent direct photoexcitation of carriers from either a band-to-band or impurity-to-band transition, and therefore, any other donor-to-acceptor pair and single-photon emission lines originating from intra-defect transitions can be precluded. Vertical photoconductive structures were fabricated to facilitate PES measurements, as schematically illustrated in the inset of Fig. 3(a). To ensure sufficient optical absorption and adequate photocurrent signals for below-bandgap photons, the AlN:Zr active layer thickness was increased to 20 μm. Fabrication began with MOCVD growth of a 0.3-μm-thick Si-doped n-$Al_{0.4}Ga_{0.6}N$ bottom contact layer on the bulk AlN substrate. To expose this bottom n-$Al_{0.4}Ga_{0.6}N$ contact layer, one-half of the sample was masked with a sapphire shadow mask prior to the subsequent growth of the 20-μm AlN:Zr active layer and a 0.3-μm Si-doped n-$Al_{0.4}Ga_{0.6}N$ top contact layer. Following sapphire mask removal, standard photolithography and inductively coupled plasma reactive-ion etching were used to define the top contact geometry, isolating it from the bottom layer. The use of a sapphire mask during growth allows us to avoid deep etching of AlN, which is highly challenging. Ohmic contact stacks comprising Ti/Al/Ti/Au were then deposited via electron-beam evaporation onto both n-type contact layers. This vertical architecture enables back-side optical excitation through the transparent bulk AlN substrate, minimizing top-metal shadowing while directing the electric field strictly across the AlN:Zr active layer. For comparison, photoconductive structures were also fabricated from a reference undoped AlN epilayer.

Dark current–voltage (I–V) characteristic of the AlN:Zr sample is shown in the inset of Fig. 3(a) and reveals a dark current of about 25 nA at 300 V and a dark electrical resistivity of ~$10^9\,\Omega$ cm, confirming the excellent electrical isolation required for low off-state leakage. A laser-driven light source coupled with a triple grating monochromator was used as a variable wavelength excitation source, providing an excitation wavelength range between 190 and 2400 nm and an optical power of about 0.2 mW. Figure 3(a) shows the PES spectrum of AlN:Zr under back-side illumination, measured at 300 V. The broad onset near 5.9 eV corresponds to fundamental band-to-band absorption. Additionally, sub-bandgap illumination resolves three distinct, prominent absorption features centered near 1.5, 1.9, and 2.8 eV. In comparison, the PES of undoped AlN epilayer shown in Fig. 3(b) exhibits a sharp photocurrent peak near the bandgap with no other visible defect transitions.

Based on first-principles calculation results[13] and its absence in the reference sample of undoped AlN epilayer, we assign the 1.5 eV peak to the direct photoexcitation of electrons from the neutral donor state $(Zr_{Al})^0$ into the conduction band. We propose that the spectral peak near 1.9 eV, which is absent in the reference sample, is due to the photoexcitation of an electron bound to a negatively charged complex of $(Zr_{Al}–V_N)^{1-}$ to the CBM. Though the excitation energy of $(Zr_{Al}–V_N)^{-1}$ to the CBM was not calculated, it should be less than 3.07 eV, since the calculated excitation energy of $(Zr_{Al}–V_N)^0$ to the CBM is 3.07 eV. The stability of this negatively charged state is mediated by the fact that the calculated energy level of this state is slightly below the energy level of Zr_{Al} donors. The absorption peak near 2.8 eV is reasonably close to the predicted energy of 3.07 eV required to excite an electron from a neutral complex of $(Zr_{Al}–V_N)^0$ to the CBM.[13] Since the concentration of $(Zr_{Al}–V_N)^0$ is expected to be lower than that of $(Zr_{Al}–V_N)^{-1}$, the photocurrent peak associated with $(Zr_{Al}–V_N)^0$ should be weaker than that of $(Zr_{Al}–V_N)^{-1}$. Experimental results in Fig. 3(a) corroborate this expectation. However, a separate first-principles calculation study revealed that valence band photoexcitation to $(V_{Al}–O_N)^{1-}$, described by the process of $(V_{Al}–O_N)^{1-} + h\nu\,(2.94\,eV) \rightarrow h^+ + (V_{Al}–O_N)^{2-}$, can yield an absorption peak at 2.94 eV.[24] Therefore, it is also plausible that the PES peaks of the AlN:Zr sample near 2.8 and 3.0 eV originate from these defect complexes, even though they are absent in the undoped AlN epilayer. Furthermore, a weak absorption footprint near 4.0 eV shown in Fig. 3(a) also aligns with the predicted optical ionization threshold of 3.97 eV for electrons bound to $(V_{Al}–O_N)^{2-}$ defect complex into the conduction band.[26] It is worth noting that the broad peak near 1.78 eV observed in the optical absorption spectrum[23] is absent in the PES of the AlN:Zr sample. This implies that the previous

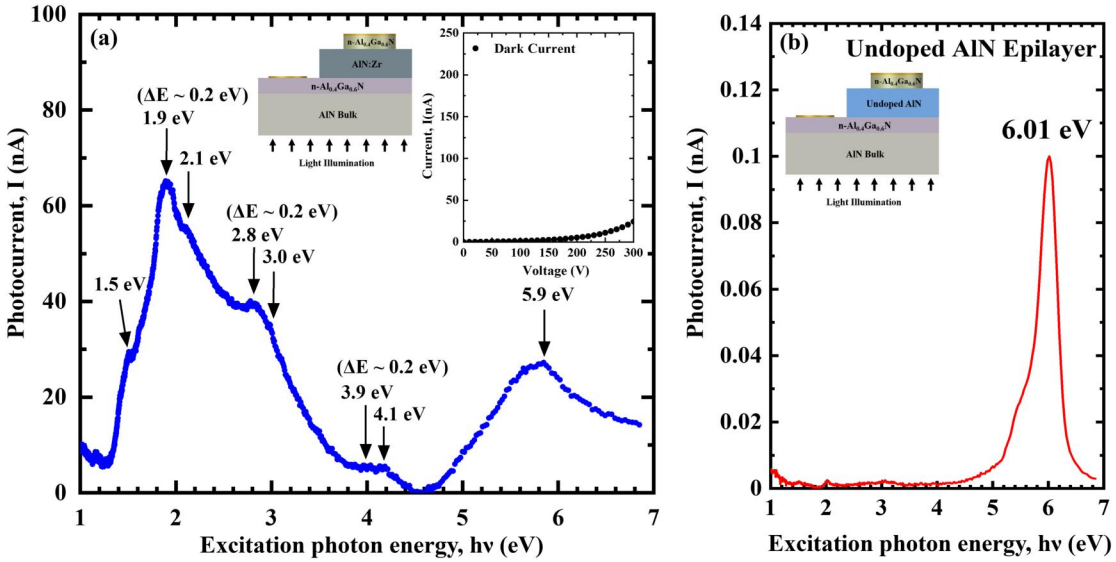

FIG. 3. (a) Photocurrent excitation spectroscopy (PES) of an AlN:Zr photoconductive device measured at V = 300 V under back-side illumination. Insets are the schematic cross-sectional view and dark I–V characteristic of the AlN:Zr device. (b) PES of the undoped AlN epilayer. Inset is the schematic cross-sectional view of the undoped AlN device.

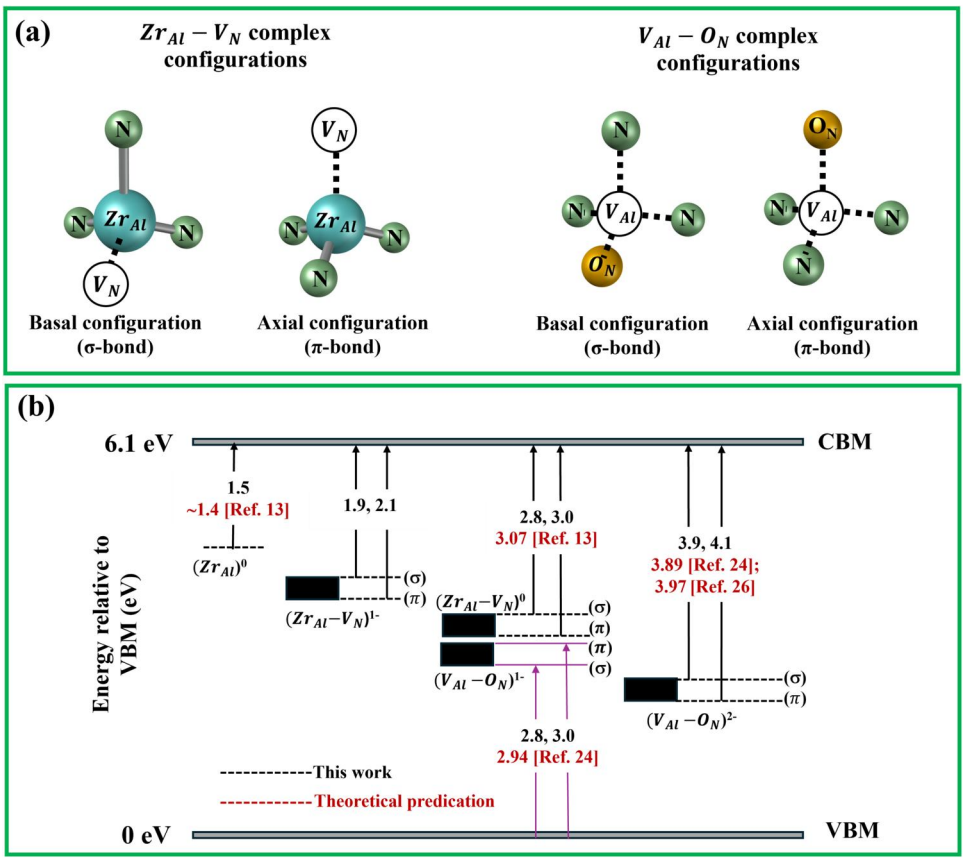

FIG. 4. (a) Illustration of atomic configurations of Zr_{Al}–V_N and V_{Al}–O_N complexes in both basal configuration (σ-bond) and axial configuration (π-bond). (b) Proposed defect-level diagram constructed from the measured transition energies observed in Fig. 3, shown by black dashed lines, which are compared with theoretical values shown in red and are considered as possible origins of the sub-bandgap photo-response features observed in Fig. 3. The presence of both σ-bonding and π-bonding configurations of Zr_{Al}–V_N and V_{Al}–O_N complexes is proposed to be responsible for the observed absorption peak doublets. For the photocurrent peak near 2.9 eV, two possible optical excitation mechanisms are included.

assignment of this optical absorption peak to optical excitation of an electron bound to a $(Zr_{Al}–V_N)^{-1}$ to the CBM needs to be rectified. A peak appearing in optical absorption spectrum but not in PES suggests that this peak is either a donor–acceptor type or an intra-defect transition involving a Zr-related defect.

Careful inspection of the PES of AlN:Zr features reveals that each sub-bandgap absorption peak, except the line involving isolated $(Zr_{Al})^0$, appears as a distinct doublet. The 1.9 eV peak features a side peak at 2.1 eV; the 2.8 eV peak pairs with an absorption shoulder at 3.0 eV; and the 4.0 eV feature splits into distinct components at 3.9 and 4.1 eV. This fine structure stems from the unique symmetry of the wurtzite AlN lattice. As illustrated in Fig. 4(a), two structural configurations exist for axial complexes: a longer single bond directed parallel to the c-axis (π-bond configuration) and three equivalent, shorter basal plane bonds (σ-bond configuration). Consequently, both ($Zr_{Al}–V_N$) and ($V_{Al}–O_N$) complexes form two distinct geometrical arrangements with unique binding energies. The energy splitting observed within these doublets is close to the known binding energy difference between π-type and σ-type configurations for complexes in GaN (0.16 eV).[27] The lower-energy, higher-intensity peaks correspond to the σ-type configurations due to their higher structural degeneracy and larger binding energy.[28] Similar doublet transition lines associated with σ-type and π-type ($V_{III}–O_N$) defect complexes have been experimentally observed in PL emission spectra of GaN[29] and AlN.[24]

The comprehensive energy level scheme extracted from our PES measurements is summarized in Fig. 4(b). For high-power extrinsic PCSS applications, all three major absorption features can be utilized for optical switching. However, our photocurrent transport measurements indicate that the optimal trigger photon energy sits around 1.9 eV, balancing high absorption efficiency with deep-level stability.

In summary, high-quality AlN:Zr epilayers were synthesized on bulk AlN substrate via MOCVD. Structural and morphologic evaluations confirmed excellent crystalline orientation and sub-nanometer surface roughness. While emission spectra were dominated by Al vacancies and their complexes with oxygen impurities, photocurrent excitation spectroscopy mapped Zr-related deep-level donor and donor-defect complex states. We resolved the isolated donor level at 1.5 eV alongside the $(Zr_{Al}–V_N)^{0/1-}$ complex configurations. Each complex exhibits a clear 0.2 eV doublet splitting driven by π-bonding and σ-bonding configurations in the wurtzite lattice. These findings experimentally confirm the deep-level electronic properties of Zr in AlN. Beyond advancing our fundamental understanding of transition-metal defects in wide-bandgap semiconductors, the results establish a robust material platform for high-efficiency extrinsic photoconductive semiconductor switches for power electronics and scalable, room-temperature quantum qubits for quantum information science.

The information, data, or work presented herein was funded in part by the Advanced Research Projects Agency-Energy (ARPA-E), U.S. Department of Energy, under ULTRAFAST program, Award No. DE-AR0001821, monitored by Dr. Johan Enslin, Dr. Olga Spahn, and Dr. Eric Carlson. The views and opinions of authors expressed herein do not necessarily state or reflect those of the United States Government or any agency thereof. Jiang and Lin are grateful to the AT&T Foundation for the support of Ed. Whitacre and Linda Whitacre endowed chairs.

AUTHOR DECLARATIONS

Conflict of Interest

The authors have no conflicts to disclose.

Author Contributions

F. A. Rafi: Data curation (equal); Formal analysis (equal); Investigation (equal); Methodology (equal); Software (equal); Validation (equal); Visualization (equal); Writing – original draft (equal); Writing – review & editing (equal). **H. Alwan:** Data curation (equal); Formal analysis (equal); Investigation (equal); Methodology (equal); Software (equal); Validation (equal); Visualization (equal); Writing – review & editing (equal). **J. Li:** Data curation (equal); Formal analysis (equal); Investigation (equal); Methodology (equal); Project administration (equal); Resources (equal); Software (equal); Supervision (equal); Validation (equal); Visualization (equal). **J. Y. Lin:** Conceptualization (equal); Formal analysis (equal); Funding acquisition (equal); Investigation (equal); Methodology (equal); Project administration (equal); Resources (equal); Supervision (equal); Validation (equal); Visualization (equal); Writing – original draft (equal); Writing – review & editing (equal). **H. X. Jiang:** Conceptualization (equal); Formal analysis (equal); Funding acquisition (equal); Investigation (equal); Methodology (equal); Project administration (equal); Resources (equal); Supervision (equal); Validation (equal); Visualization (equal); Writing – original draft (equal); Writing – review & editing (equal).

DATA AVAILABILITY

The data that support the findings of this study are available within the article.

REFERENCES

[1]J. Li, K. B. Nam, M. L. Nakarmi, J. Y. Lin, H. X. Jiang, P. Carrier, and S.-H. Wei, "Band structure and fundamental optical transitions in wurtzite AlN," Appl. Phys. Lett. **83**, 5163 (2003).
[2]K. B. Nam, J. Li, M. L. Nakarmi, J. Y. Lin, and H. X. Jiang, "Unique optical properties of AlGaN alloys and related ultraviolet emitters," Appl. Phys. Lett. **84**, 5264 (2004).
[3]Y. Taniyasu, M. Kasu, and T. Makimoto, "An aluminium nitride light-emitting diode with a wavelength of 210 nanometres," Nature **441**, 325 (2006).
[4]M. A. Khan, K. Balakrishnan, and T. Katona, "Ultraviolet light-emitting diodes based on group three nitrides," Nat. Photonics **2**, 77 (2008).
[5]Z. Zhang, M. Kushimoto, T. Sakai, N. Sugiyama, L. J. Schowalter, C. Sasaoka, and H. Amano, "A 271.8 nm deep-ultraviolet laser diode for room temperature operation," Appl. Phys. Express **12**, 124003 (2019).
[6]Q. Wang, S. Zhao, A. Connie, I. Shih, Z. Mi, T. Gonzalez, M. Andrews, X. Du, J. Y. Lin, and H. X. Jiang, "Optical properties of strain-free AlN nanowires grown by molecular beam epitaxy on Si substrates," Appl. Phys. Lett. **104**, 223107 (2014).
[7]W. A. Doolittle, C. M. Matthews, H. Ahmad, K. Motoki, S. Lee, A. Ghosh, E. N. Marshall, A. L. Tang, P. Manocha, and P. D. Yoder, "Prospectives for AlN electronics and optoelectronics and the important role of alternative synthesis," Appl. Phys. Lett. **123**, 070501 (2023).
[8]M. Higashiwaki, R. Kaplar, J. Pernot, and H. Zhao, "Ultrawide bandgap semiconductors," Appl. Phys. Lett. **118**, 200401 (2021).
[9]M. A. Khan, A. Bhattarai, J. N. Kuznia, and D. T. Olson, "High electron mobility transistor based on GaN-$Al_xGa_{1-x}N$ heterojunction," Appl. Phys. Lett. **63**, 1214 (1993).
[10]Y. H. Chen, J. Encomendero, C. Savant, V. Protasenko, H. G. Xing, and D. Jena, "Electron mobility enhancement by electric field engineering of AlN/

GaN/AlN quantum-well HEMTs on single-crystal AlN substrates," Appl. Phys. Lett. **124**, 152111 (2024).
[11]M. Hiroki, Y. Taniyasu, and K. Kumakura, "High-temperature performance of AlN MESFETs with epitaxially *n*-type AlN grown channel layers," IEEE Electron Device Lett. **43**, 350 (2022).
[12]T. Kumabe, A. Yoshikawa, S. Kawasaki, M. Kushimoto, Y. Honda, M. Arai, J. Suda, and H. Amano, "Demonstration of AlGaN-on-AlN pn diodes with dopant-free distributed polarization doping," IEEE Trans. Electron Devices **71**, 3396 (2024).
[13]J. B. Varley, A. Janotti, and C. G. Van de Walle, "Defects in AlN as candidates for solid-state qubits," Phys. Rev. B **93**, 161201(R) (2016).
[14]A. Aghdaei, R. Pandiyan, B. Ilahi, M. Chicoine, M. El Gowini, F. Schiettekatte, L. G. Fréchette, and D. Morris, "Engineering visible light emitting point defects in Zr-implanted polycrystalline AlN films," J. Appl. Phys. **128**, 245701 (2020).
[15]A. Senichev, Z. O. Martin, Y. Wang, O. M. Matthiessen, A. Lagutchev, H. Htoon, A. Boltasseva, and V. M. Shalaev, "Quantum emitters in aluminum nitride induced by heavy ion irradiation," APL Quantum **1**, 036103 (2024).
[16]P. B. Perry and R. F. Rutz, "The optical absorption edge of single-crystal AlN prepared by a close-spaced vapor process," Appl. Phys. Lett. **33**, 319 (1978).
[17]G. A. Slack, "Nonmetallic crystals with high thermal conductivity," J. Phys. Chem. Solids **34**, 321 (1973).
[18]R. L. Xu, M. M. Rojo, S. M. Islam, A. Sood, B. Vareskic, A. Katre, N. Mingo, K. E. Goodson, H. G. Xing, D. Jena, and E. Pop, "Thermal conductivity of crystalline AlN and the influence of atomic-scale defects," J. Appl. Phys. **126**, 185105 (2019).
[19]Z. Cheng, Y. R. Koh, A. Mamun, J. Shi, T. Bai, K. Huynh, L. Yates, Z. Liu, and R. Li, "Experimental observation of high intrinsic thermal conductivity of AlN," Phys. Rev. Mater. **4**, 044602 (2020).
[20]Y. Taniyasu, M. Kasu, and T. Makimoto, "Increased electron mobility in *n*-type Si-doped AlN by reducing dislocation density," Appl. Phys. Lett. **89**, 182112 (2006).
[21]T. L. Chu and R. W. Kelm, "The preparation and properties of aluminum nitride films," J. Electrochem. Soc. **122**, 995 (1975).
[22]H. Alwan, N. K. Hossain, J. Li, J. Y. Lin, and H. X. Jiang, "Growth and characterization of high-quality Zr doped AlN epilayers," Appl. Phys. Lett. **126**, 022106 (2025).
[23]H. Alwan, M. Almohammad, J. Li, J. Y. Lin, and H. X. Jiang, "Optical properties of Zr-doped AlN epilayers," APL Mater. **13**, 071115 (2025).
[24]Q. Zhou, Z. Zhang, H. Li, S. Golovynskyi, X. Tang, H. Wu, J. Wang, and B. Li, "Below bandgap photoluminescence of an AlN crystal: Co-existence of two different charging states of a defect center," APL Mater. **8**, 081107 (2020).
[25]N. Nepal, M. L. Nakarmi, J. Y. Lin, and H. X. Jiang, "Photoluminescence studies of impurity transitions in AlGaN alloys," Appl. Phys. Lett. **89**, 092107 (2006).
[26]Q. Yan, A. Janotti, M. Scheffler, and C. G. Van de Walle, "Origins of optical absorption and emission lines in AlN," Appl. Phys. Lett. **105**, 111104 (2014).
[27]K. L. Jablonska, T. Suski, I. Gorczyca, N. E. Christensen, K. E. Attenkofer, R. C. C. Perera, E. M. Gullikson, J. H. Underwood, D. L. Ederer, and Z. L. Weber, "Electronic states in valence and conduction bands of group-III nitrides: Experiment and theory," Phys. Rev. B **61**, 16623 (2000).
[28]J. Neugebauer and C. G. Van de Walle, "Gallium vacancies and the yellow luminescence in GaN," Appl. Phys. Lett. **69**, 503 (1996).
[29]A. Sedhain, J. Li, J. Y. Lin, and H. X. Jiang, "Nature of deep center emissions in GaN," Appl. Phys. Lett. **96**, 151902 (2010).